ELSEVIER

Mathematics and Computers in Simulation 52 (2000) 273–287

MATHEMATICS AND COMPUTERS IN SIMULATION

www.elsevier.nl/locate/matcom

Quasi-hydrodynamic modelling and computer simulation of coupled thermo-electrical processes in semiconductors

R.V.N. Melnik [a,*], Hao He [b]

[a] *CSIRO Mathematical & Information Sciences, Macquarie University Campus, North Ryde, Sydney, NSW 2113, Australia*

[b] *Department of Theoretical Physics, School of Physics, University of Sydney, Sydney NSW 2006, Australia*

Received 1 January 2000; accepted 1 April 2000

Abstract

The quasi-hydrodynamic model for semiconductor devices is a typical example of non-local models which, in contrast to the conventional drift-diffusion models, allows to account for non-equilibrium processes in semiconductor plasma. In this paper, we present results of a numerical simulation of semiconductor devices using the quasi-hydrodynamic model. The results have been obtained with the package SCSIMU, a C++ based program in which efficient exponential difference schemes for the quasi-hydrodynamic model have been implemented. Algorithmic procedures and modelling of realistic semiconductor devices such as ballistic and PIN diodes are discussed with numerical results.

Keywords: Semiconductor device simulation; Quasi-hydrodynamic models; Exponential difference schemes
Subj. Class. 35Q72; 65M06; 73V15

1. Introduction

The quasi-hydrodynamic model for semiconductor device simulation plays an intermediate role between Boltzman's type models and drift-diffusion models. While the latter models are known to be insufficient for the description of non-local and non-equilibrium processes in semiconductor plasma, the high computational cost and 'noisiness' (with a great deal of redundant information) of Boltzman models preclude their effective use in engineering practice. Therefore, the development of computational software for quasi-hydrodynamic type models constitutes an important and challenging task for the engineering simulation of semiconductor devices. The basis of our current deliberations is the following quasi-hydrodynamic model:

* Corresponding author. Tel.: +61-2-9325-3247; fax: +61-2-9325-3200.
E-mail address: roderick.melnik@cmis.csiro.au (H. He)

PII: S0378-4754(00)00161-0

$$\begin{cases} \partial_{xx}\varphi = \dfrac{q(n-p-N)}{\epsilon\epsilon_0}, \\ \partial_t n - \partial_x J_\mathrm{n}/q = F, \\ \partial_t p + \partial_x J_\mathrm{p}/q = F, \\ \partial_t \bar{\mathcal{E}}_\mathrm{n} + \partial_x Q_\mathrm{n} = -J_\mathrm{n}\partial_x\varphi + P_\mathrm{n}, \\ \partial_t \bar{\mathcal{E}}_\mathrm{p} + \partial_x Q_\mathrm{p} = -J_\mathrm{p}\partial_x\varphi + P_\mathrm{p}, \end{cases} \tag{1.1}$$

where n and p are concentrations of the majority (electrons) and minority (holes) carriers, respectively, φ is the electrostatic potential, F is the generation/recombination/ionisation term, P_n and P_p are the rates of energy loss (by scattering on the lattice) for electrons and holes, respectively, J_n and J_p are the current densities, Q_n and Q_p are the energy fluxes, N is the doping density of the device (the summarised concentration of dopants), q is the electron charge, ϵ and ϵ_0 are the relative dielectric permittivities of the semiconductor material and of vacuum, respectively, $\bar{\mathcal{E}}_\mathrm{n}$ and $\bar{\mathcal{E}}_\mathrm{p}$ are approximate energy densities of the carriers. The following relationships supplement system (1.1):

$$\bar{\mathcal{E}}_\mathrm{n} = 1.5nT_\mathrm{n}, \quad \bar{\mathcal{E}}_\mathrm{p} = 1.5pT_\mathrm{p}, \quad P_\mathrm{n} = \frac{n(T_\mathrm{l}-T_\mathrm{n})}{\tau_\omega^\mathrm{n}}, \quad P_\mathrm{p} = \frac{p(T_\mathrm{l}-T_\mathrm{p})}{\tau_\omega^\mathrm{p}}, \tag{1.2}$$

$$D_\mathrm{n} = \mu_\mathrm{n}T_\mathrm{n}, \quad D_\mathrm{p} = \mu_\mathrm{p}T_\mathrm{p}, \quad \mu_\mathrm{n} = \mu_\mathrm{n}^0\sqrt{\frac{T_\mathrm{n}}{T_\mathrm{l}}}, \quad \mu_\mathrm{p} = \mu_\mathrm{p}^0\sqrt{\frac{T_\mathrm{p}}{T_\mathrm{l}}}, \tag{1.3}$$

$$J_\mathrm{n} = -qn\mu_\mathrm{n}\partial_x\varphi + \partial_x(T_\mathrm{n}\mu_\mathrm{n}n), \quad J_\mathrm{p} = -qp\mu_\mathrm{p}\partial_x\varphi - \partial_x(T_\mathrm{p}\mu_\mathrm{p}p), \tag{1.4}$$

$$Q_\mathrm{n} = \beta_\mathrm{n}T_\mathrm{n}n\mu_\mathrm{n}\partial_x\varphi - \frac{\beta_\mathrm{n}\partial_x[T_\mathrm{n}D_\mathrm{n}n]}{q}, \quad Q_\mathrm{p} = -\beta_\mathrm{p}T_\mathrm{p}p\mu_\mathrm{p}\partial_x\varphi - \frac{\beta_\mathrm{p}\partial_x[T_\mathrm{p}D_\mathrm{p}p]}{q}, \tag{1.5}$$

where T_n and T_p are the carrier temperatures, T_l is the lattice temperature, τ_ω^n and τ_ω^p are average energy relaxation times (s) for electrons and holes, respectively, D_n (D_p) and μ_n (μ_p) are the diffusion and mobility coefficients (cm^2/Vs). Note that the current densities can be equivalently defined as follows:

$$J_\mathrm{n} = -qnv_\mathrm{n} \quad \text{and} \quad J_\mathrm{p} = qpv_\mathrm{p}, \tag{1.6}$$

which provide us with formulae for computing carrier velocities, v_n and v_p. For simplicity, the Peltier coefficients, β_n and β_p are assumed to be constants equal to 2.5 and for the energy relaxation times we use the following formulae:

$$\tau_\omega^\mathrm{n} = \frac{3\mu_\mathrm{n}^0\sqrt{T_\mathrm{l}T_\mathrm{n}}}{2q(v_\mathrm{s}^\mathrm{n})^2}, \quad \mu_\mathrm{n}^0 = 1400 \quad \text{and} \quad \tau_\omega^\mathrm{p} = \frac{3\mu_\mathrm{p}^0\sqrt{T_\mathrm{l}T_\mathrm{p}}}{2q(v_\mathrm{s}^\mathrm{p})^2}, \quad \mu_\mathrm{p}^0 = 400, \tag{1.7}$$

where v_s^n and v_s^p are saturation velocities of carriers. The recombination term F is given by

$$F(n,p) = \frac{pn - n_\mathrm{ie}^2}{\tau_\mathrm{n}(p+n_\mathrm{ie}) + \tau_\mathrm{p}(n+n_\mathrm{ie})}, \tag{1.8}$$

where n_ie is the effective intrinsic concentration of carriers and the carrier life times are set as follows:

$$\tau_\mathrm{n} = 1.7\times10^{-5}, \quad \tau_\mathrm{p} = 3.95\times10^{-4}.$$

Initial and boundary conditions for problems (1.1)–(1.8) are device specific. For the sake of technical convenience, we write the problem in terms of dimensionless variables (keeping the same notation as in (1.1)–(1.8)):

$$\begin{cases} \partial_{xx}\varphi = n - p - N, \\ \partial_t n - \partial_x J_{\mathrm{n}} = F, \\ \partial_t p + \partial_x J_{\mathrm{p}} = F, \\ 3/2\partial_t(nT_{\mathrm{n}}) + \partial_x Q_{\mathrm{n}} = -J_{\mathrm{n}}\partial_x\varphi + P_{\mathrm{n}}, \\ 3/2\partial_t(pT_{\mathrm{p}}) + \partial_x Q_{\mathrm{p}} = -J_{\mathrm{p}}\partial_x\varphi + P_{\mathrm{p}}, \end{cases} \tag{1.9}$$

where

$$J_{\mathrm{n}} = -n\mu_{\mathrm{n}}\partial_x\varphi + \partial_x(T_{\mathrm{n}}\mu_{\mathrm{n}}n), \quad J_{\mathrm{p}} = -p\mu_{\mathrm{p}}\partial_x\varphi - \partial_x(T_{\mathrm{p}}\mu_{\mathrm{p}}p), \tag{1.10}$$

$$Q_{\mathrm{n}} = \beta_{\mathrm{n}}T_{\mathrm{n}}n\mu_{\mathrm{n}}\partial_x\varphi - \beta_{\mathrm{n}}\partial_x[T_{\mathrm{n}}D_{\mathrm{n}}n], \quad Q_{\mathrm{p}} = -\beta_{\mathrm{p}}T_{\mathrm{p}}p\mu_{\mathrm{p}}\partial_x\varphi - \beta_{\mathrm{p}}\partial_x[T_{\mathrm{p}}D_{\mathrm{p}}p]. \tag{1.11}$$

2. Semiconductor devices used in numerical experiments

To solve the coupled system partial differential equations (1.9)–(1.11), we developed an efficient C++ code, which is easily adaptable for a wide range of semiconductor devices. In this paper, we present results of the simulation for two types of devices. The typical representative of the first type is the silicon-based $p^+ - i - n^+$ (PIN) diode used extensively for microwave control applications such as microwave switches and for electronically steered phased-array antennas [3]. The length of the simulated diode is chosen to be 3.5 μm (see also [3]). The p^+ region of length 0.5 μm is doped at density -10^{18} cm^{-3}. The central region of length 2.0 μm is doped at density 3.5×10^{14} cm^{-3}, while the n^+ region is doped at 2.4×10^{19} cm^{-3}. A schematic doping profile of this device is shown in Fig. 1(a).

The typical representative of the other type of devices is the $n^+ - n - n^+$ ballistic diode [1,2]. This device is often used to model the $n^+ - n - n^+$ channel in MEtal-Semiconductor Field-Effect Transistors (MESFET). The simulated diode has a central n region of length 0.4 μm bounded by two n^+ regions of

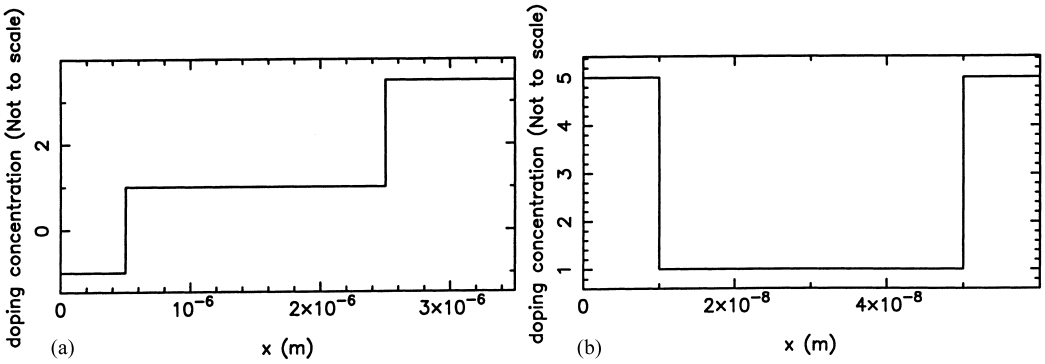

Fig. 1. Doping distribution in semiconductor structure. (a) PIN diode; (b) ballistic diode.

length 0.1 μm each. The n^+ regions are doped at density $N = 5 \times 10^{17}\,\mathrm{cm}^{-3}$, while the n region is doped at $N = 2 \times 10^{15}\,\mathrm{cm}^{-3}$. We show the schematic doping profile for this device in Fig. 1(b).

3. Numerical approximations

In this section we briefly describe the main ideas of our numerical scheme for the stationary case.

3.1. Discretisation of the Poisson equation

For the solution of the Poisson equation

$$\partial_{xx}\varphi = n - p - N, \tag{3.1}$$

we use the following discretisation:

$$\mathcal{F}_i^{\varphi}(\varphi_{i-1}^{l+1}, \varphi_i^{l+1}, \varphi_{i+1}^{l+1}) = \frac{(\varphi_{i+1}^{l+1} - \varphi_i^{l+1})}{h_{i+1}} - \frac{(\varphi_i^{l+1} - \varphi_{i-1}^{l+1})}{h_i} - h_i^*[n_i^l \exp(\varphi_i^{l+1} - \varphi_i^l) - p_i^l \exp(-\varphi_i^{l+1} + \varphi_i^l) - N] = 0. \tag{3.2}$$

Note that in this discretisation we used the relationships $n^{l+1} = n^l \exp(\varphi^{l+1} - \varphi^l)$ and $p^{l+1} = p^l \exp(\varphi^l - \varphi^{l+1})$ (written in normalised units), easily obtainable under the assumption of constant carrier temperatures. Then, the Jacobian of system (3.2) is determined by the following partial derivatives:

$$\frac{\partial \mathcal{F}_i^{\varphi}}{\partial \varphi_{i-1}^{l+1}} = \frac{1}{h_i}, \quad \frac{\partial \mathcal{F}_i^{\varphi}}{\partial \varphi_{i+1}^{l+1}} = \frac{1}{h_{i+1}}, \tag{3.3}$$

$$\frac{\partial \mathcal{F}_i^{\varphi}}{\partial \varphi_i^{l+1}} = -\frac{1}{h_{i+1}} - \frac{1}{h_i} - h_i^*(n_i^l \exp(\varphi_i^{l+1} - \varphi_i^l) + p_i^l \exp(-\varphi_i^{l+1})). \tag{3.4}$$

The banded structure of this Jacobian permits an efficient computational implementation of the linearised system using a sparse solver. Indeed, approximations to each non-linear equation of system (1.9) can be written in the form

$$\vec{\mathcal{F}}(\boldsymbol{x}) = 0, \tag{3.5}$$

where $\vec{\mathcal{F}}$ is an equation-specific discrete operator and $\boldsymbol{x}$ is a quantity to be determined (say, φ). We start with an initial approximate solution $\boldsymbol{x}'$ and solve the following system of linear equations:

$$\boldsymbol{J} \cdot \delta\boldsymbol{x} = -\vec{\mathcal{F}}(\boldsymbol{x}'), \tag{3.6}$$

with the Jacobian of the system (that is a sparse matrix) given by

$$J_{ij} = \frac{\partial \mathcal{F}_i}{\partial x_j}. \tag{3.7}$$

The values of $\boldsymbol{x}'$ are then updated according to the standard methodology

$$\boldsymbol{x}'_{\mathrm{new}} \leftarrow \boldsymbol{x}'_{\mathrm{old}} + \delta\boldsymbol{x} \tag{3.8}$$

and steps (3.6)–(3.8) are repeated until the required accuracy is achieved.

3.2. Discretisation of the continuity equations

We use exponential difference schemes for the discretisation of continuity equations. In the stationary case these equations have the form

$$-\partial_x J_{\rm n} = F, \quad \text{where} \quad J_{\rm n} = -n\mu_{\rm n}\partial_x\varphi + \partial_x(T_{\rm n}\mu_{\rm n} n), \tag{3.9}$$

$$\partial_x J_{\rm p} = F, \quad \text{where} \quad J_{\rm p} = -p\mu_{\rm p}\partial_x\varphi - \partial_x(T_{\rm p}\mu_{\rm p} p). \tag{3.10}$$

Eq. (3.9) is discretised as follows:

$$\vec{\mathcal{F}}_i^{\rm n} = A_i^{\rm n} n_{i-1}^{l+1} + B_i^{\rm n} n_{i+1}^{l+1} - C_i^{\rm n} n_i^{l+1} + h_i^* F_i(n_i^{l+1}, p_i) = 0, \tag{3.11}$$

where

$$A_i^{\rm n} = \frac{D_{\rm n}[(T_{\rm n})_{i-1}^{l+1}]}{h_i} f\left(\frac{\varphi_i^{l+1} - \varphi_{i-1}^{l+1}}{(T_{\rm n})_{i-1}^{l+1}}\right), \tag{3.12}$$

$$B_i^{\rm n} = \frac{D_{\rm n}[(T_{\rm n})_{i+1}^{l+1}]}{h_{i+1}} f_1\left(\frac{\varphi_{i+1}^{l+1} - \varphi_i^{l+1}}{(T_{\rm n})_{i+1}^{l+1}}\right), \quad C_i^{\rm n} = A_{i+1}^{\rm n} + B_{i-1}^{\rm n}. \tag{3.13}$$

The Jacobian of system (3.11) is determined by

$$\frac{\partial\mathcal{F}_i^{\rm n}}{\partial n_{i-1}^{l+1}} = A_i^{\rm n}, \quad \frac{\partial\mathcal{F}_i^{\rm n}}{\partial n_i^{l+1}} = -C_i^{\rm n} + h_i^*\frac{\partial F_i}{\partial n_i^{l+1}}, \quad \frac{\partial\mathcal{F}_i^{\rm n}}{\partial n_{i+1}^{l+1}} = B_i^{\rm n}. \tag{3.14}$$

Similarly, we obtain the discretised equation and the Jacobian for the continuity Eq. (3.10):

$$\mathcal{F}_i^{\rm p} = A_i^{\rm p} p_{i-1}^{l+1} + B_i^{\rm p} p_{i+1}^{l+1} - C_i^{\rm p} p_i^{l+1} + h_i^* F_i(n_i, p_i^{l+1}) = 0, \tag{3.15}$$

where

$$A_i^{\rm p} = \frac{D_{\rm p}[(T_{\rm p})_{i-1}^{l+1}]}{h_i} f_1\left(\frac{\varphi_i^{l+1} - \varphi_{i-1}^{l+1}}{(T_{\rm p})_{i-1}^{l+1}}\right), \tag{3.16}$$

$$B_i^{\rm n} = \frac{D_{\rm p}[(T_{\rm p})_{i+1}^{l+1}]}{h_{i+1}} f\left(\frac{\varphi_{i+1}^{l+1} - \varphi_i^{l+1}}{(T_{\rm p})_{i+1}^{l+1}}\right), \quad C_i^{\rm p} = A_{i+1}^{\rm n} + B_{i-1}^{\rm n}, \tag{3.17}$$

$$\partial\mathcal{F}_i^{\rm p}/\partial p_{i-1}^{l+1} = A_i^{\rm p}, \quad \frac{\partial\mathcal{F}_i^{\rm p}}{\partial p_i^{l+1}} = -C_i^{\rm p} + h_i^*\frac{\partial F_i}{\partial p_i^{l+1}}, \quad \frac{\partial\mathcal{F}_i^{\rm p}}{\partial p_{i+1}^{l+1}} = B_i^{\rm p}. \tag{3.18}$$

3.3. Discretisation of the energy balance equations

The energy balance equations are also approximated by exponential difference schemes. In the stationary case these equations have the form

$$\partial_x Q_{\rm n} = -J_{\rm n}\partial_x\varphi + P_{\rm n}, \quad \partial_x Q_{\rm p} = J_{\rm p}\partial_x\varphi + P_{\rm p}. \tag{3.19}$$

The first equation in (3.19) is approximated by the following scheme (with respect to the time layer $l+1$):

$$\mathcal{F}_i^{\mathcal{E}_\mathrm{n}} = \tilde{A}_i^\mathrm{n}(\mathcal{E}_\mathrm{n})_{i-1} + \tilde{B}_i^\mathrm{n}(\mathcal{E}_\mathrm{n})_{i+1} - \tilde{C}_i^\mathrm{n}(\mathcal{E}_\mathrm{n})_i + R_i^{\mathcal{E}_\mathrm{n}} = 0, \tag{3.20}$$

where $\mathcal{E}_\mathrm{n} = nT_\mathrm{n}$,

$$R_i^{\mathcal{E}_\mathrm{n}} = -h_i^* \left\{ -\mu_\mathrm{n}[(T_\mathrm{n})_i]\varphi_{\bar{x}\hat{x},i} - \frac{\mu_\mathrm{n}[(T_\mathrm{n})_i](\varphi_{\check{x},i})^2}{(T_\mathrm{n})_i} + \frac{1}{\tau_\omega^\mathrm{n}[(T_\mathrm{n})_i]} - \frac{1}{(\tau_\omega^\mathrm{n}[(T_\mathrm{n})_i](T_\mathrm{n})_i)} \right\} (\mathcal{E}_\mathrm{n})_i, \tag{3.21}$$

and the coefficients of this difference scheme are defined as follows:

$$(\tilde{A})_i^\mathrm{n} = \frac{\beta_\mathrm{n} D_\mathrm{n}[(T_\mathrm{n})_{i-1}^{l+1}]}{h_i} f\left(\frac{1+\beta_\mathrm{n}}{\beta_\mathrm{n}} \frac{\varphi_i^{l+1} - \varphi_{i-1}^{l+1}}{(T_\mathrm{n})_{i-1}^{l+1}} \right), \tag{3.22}$$

$$(\tilde{B})_i^\mathrm{n} = \frac{\beta_\mathrm{n} D_\mathrm{n}[(T_\mathrm{n})_{i+1}^{l+1}]}{h_{i+1}} f_1\left(\frac{1+\beta_\mathrm{n}}{\beta_\mathrm{n}} \frac{\varphi_{i+1}^{l+1} - \varphi_i^{l+1}}{(T_\mathrm{n})_{i+1}^{l+1}} \right), \quad \tilde{C}_i^\mathrm{n} = \tilde{A}_{i+1}^\mathrm{n} + \tilde{B}_{i-1}^\mathrm{n}. \tag{3.23}$$

Here we use standard difference scheme notation [5,6] such as

$$\varphi_{\bar{x}\hat{x},i} = \frac{1}{h_i^*}\left[\frac{\varphi_{i+1} - \varphi_i}{h_{i+1}} - \frac{\varphi_i - \varphi_{i-1}}{h_i} \right], \quad h_i = x_i - x_{i-1},$$

$$\varphi_{\check{x},i} = \frac{(\varphi_{i+1} - \varphi_{i-1})}{(2h_i^*)}, \quad h_i^* = \frac{(h_i + h_{i+1})}{2}.$$

Similarly, the discretised equation for holes is (at the time layer $l+1$)

$$\mathcal{F}_i^{\mathcal{E}_\mathrm{p}} = \tilde{A}_i^\mathrm{p}(\mathcal{E}_\mathrm{p})_{i-1} + \tilde{B}_i^\mathrm{p}(\mathcal{E}_\mathrm{p})_{i+1} - \tilde{C}_i^\mathrm{p}(\mathcal{E}_\mathrm{p})_i + R_i^{\mathcal{E}_\mathrm{p}} = 0 \tag{3.24}$$

where $\mathcal{E}_\mathrm{p} = pT_\mathrm{p}$,

$$R_i^{\mathcal{E}_\mathrm{p}} = -h_i^* \left\{ \mu_\mathrm{p}[(T_\mathrm{p})_i]\varphi_{\bar{x}\hat{x},i} - \frac{\mu_\mathrm{n}[(T_\mathrm{p})_i](\varphi_{\check{x},i})^2}{(T_\mathrm{p})_i} + \frac{1}{\tau_\omega^\mathrm{p}[(T_\mathrm{p})_i]} - \frac{1}{(\tau_\omega^\mathrm{p}[(T_\mathrm{p})_i](T_\mathrm{p})_i)} \right\} (\mathcal{E}_\mathrm{p})_i, \tag{3.25}$$

and the coefficients of this difference scheme are defined as follows:

$$(\tilde{A})_i^\mathrm{p} = \frac{\beta_\mathrm{p} D_\mathrm{p}[(T_\mathrm{p})_{i-1}^{l+1}]}{h_i} f_1\left(\frac{1+\beta_\mathrm{p}}{\beta_\mathrm{p}} \frac{\varphi_i^{l+1} - \varphi_{i-1}^{l+1}}{(T_\mathrm{p})_{i-1}^{l+1}} \right), \tag{3.26}$$

$$(\tilde{B})_i^\mathrm{p} = \frac{\beta_\mathrm{p} D_\mathrm{p}[(T_\mathrm{p})_{i+1}^{l+1}]}{h_{i+1}} f\left(\frac{1+\beta_\mathrm{p}}{\beta_\mathrm{p}} \frac{\varphi_{i+1}^{l+1} - \varphi_i^{l+1}}{(T_\mathrm{p})_{i+1}^{l+1}} \right), \quad \tilde{C}_i^\mathrm{p} = \tilde{A}_{i+1}^\mathrm{p} + \tilde{B}_{i-1}^\mathrm{p}. \tag{3.27}$$

In order to adequately describe physical processes in a number of semiconductor devices the splitting algorithm based upon an 'independent' solution of each non-linear equation of system (1.9) may not be appropriate. In such cases, energy balance equations have to be solved simultaneously with continuity equations leading to new challenges in the computational implementation of the proposed discrete schemes. We address these issues in Section 5.

4. Drift-diffusion approximation as an initial approximation for the solution of the quasi-hydrodynamic model

Assuming that carriers are in thermal equilibrium with the lattice and that carrier temperatures are equal to the lattice temperature, we consider the standard drift-diffusion model in the stationary case

$$\begin{cases} \partial_{xx}\varphi = n - p - N, \\ -\partial_x J_{\mathrm{n}} = F, \\ \partial_x J_{\mathrm{p}} = F. \end{cases} \tag{4.1}$$

This system provides an initial approximation for the solution of the more complicated system (1.9). We solve each equation in system (4.1) individually, so that the results from the previous equation are used for the next equation until the global convergence is reached. In order to accelerate the convergence, the Poisson equation is solved twice, in each 'semi-global' iteration after solving each continuity equation. The flowchart of the algorithm is shown in Fig. 2.

The initial approximations for the drift-diffusion model are determined by the quasi-neutrality condition

$$n_{\mathrm{ie}} \exp(V - \varphi) - n_{\mathrm{ie}} \exp(\varphi - V) + N = 0, \tag{4.2}$$

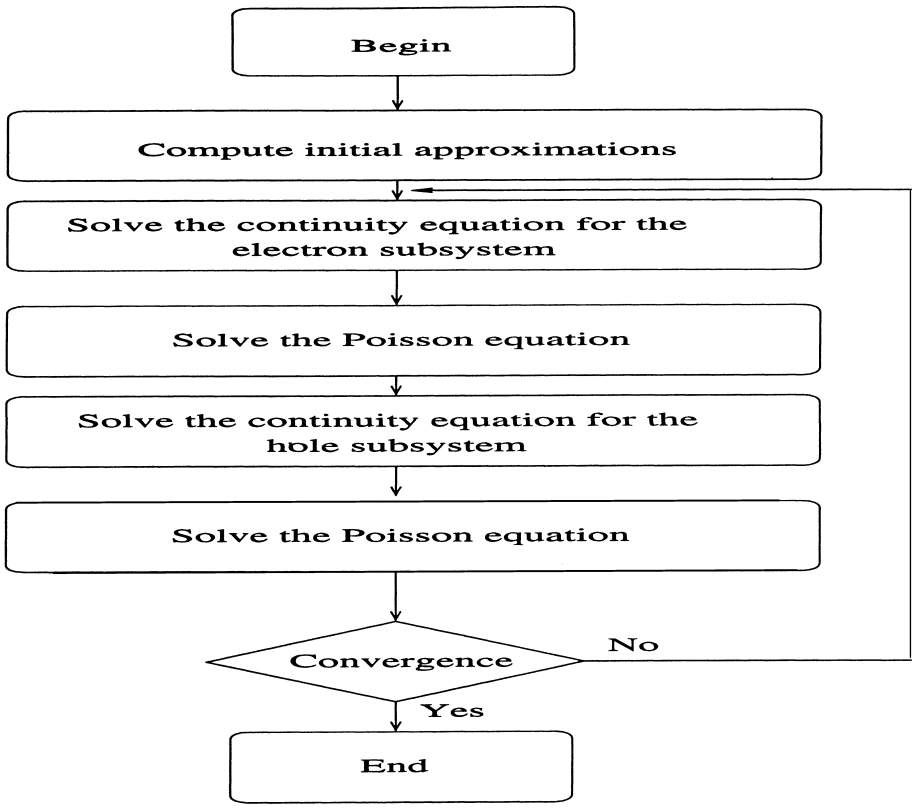

Fig. 2. Flowchart of Program 1: the solution of the drift-diffusion model.

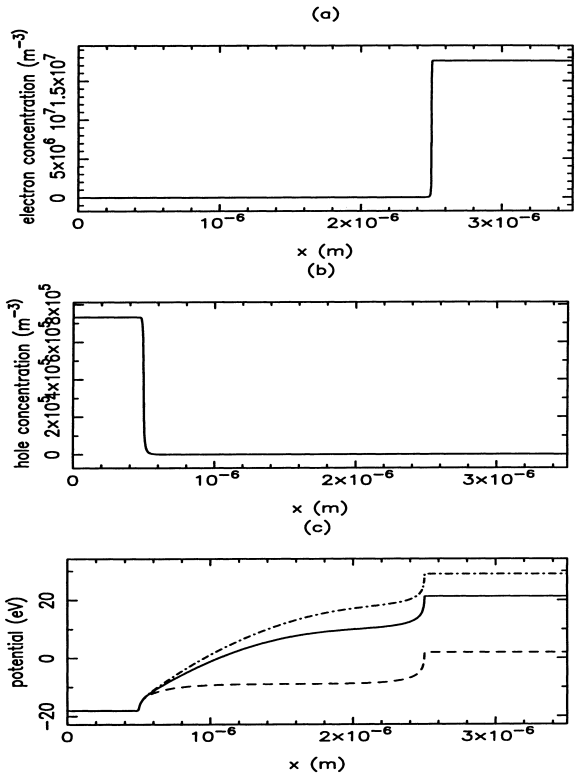

Fig. 3. Results from Program 1: (a) concentration of electrons; (b) concentration of holes; (c) potential profile (the applied voltages are $V = -0.5, 0.0, 0.2$ (dashed, solid, and dot-dashed lines, respectively).

where the initial approximation for the potential has the form

$$\varphi = V + \text{sign}(N) \ln\left(\frac{N}{n_{\text{ie}}}\right), \tag{4.3}$$

and V is the applied voltage. Then the concentrations can be determined using the Boltzmann statistics as follows:

$$n = n_{\text{ie}} \exp(\varphi), \quad p = n_{\text{ie}} \exp(-\varphi), \tag{4.4}$$

where $n_{\text{ie}} = 1.4 \times 10^{10}\ \text{cm}^{-3}$. As an example, we present in Fig. 3 the results of computation of physical characteristics of the PIN device for different applied voltages $V = -0.5, 0.0, 0.2$.

5. Computation with the quasi-hydrodynamic model

Taking the solution of the drift-diffusion model as an initial approximation, we developed a program that accounts for the effect of carrier temperatures. This program allows us to solve the full system (1.9) including the energy balance equations. From the solution of the drift-diffusion system (4.1), in a single

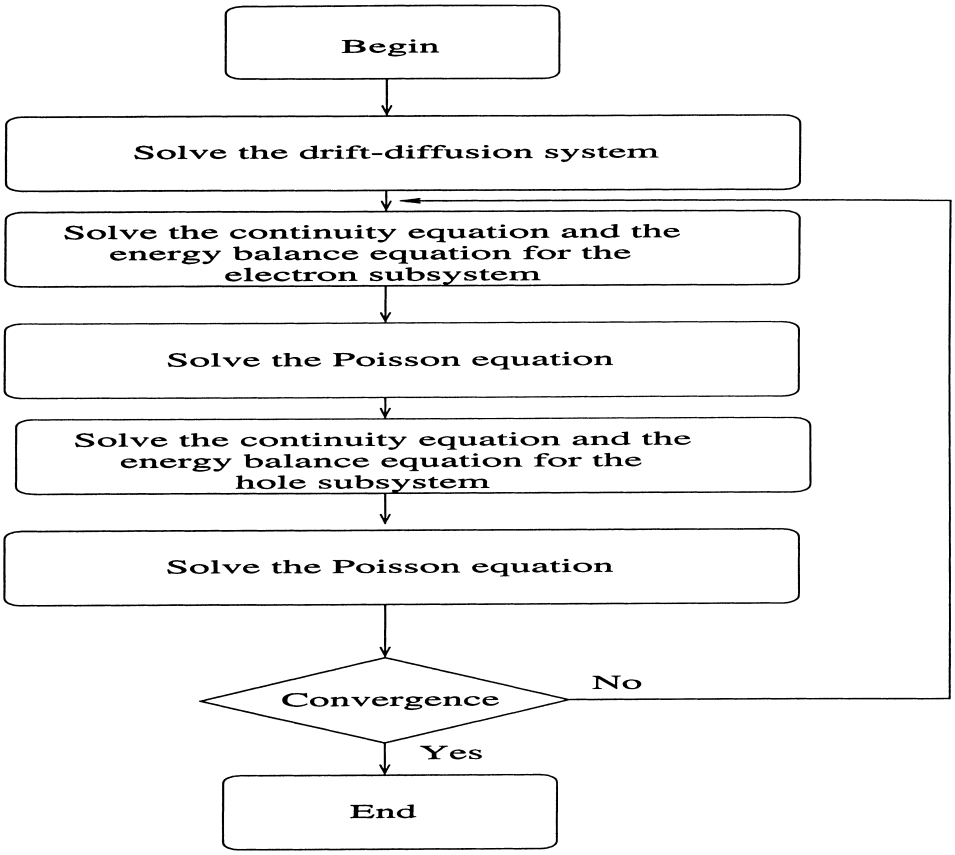

Fig. 4. Flowchart of Program 2: the solution of the quasi-hydrodynamic model.

computational block we simultaneously solve the equation of continuity and the energy balance equation for electrons. After the new potential values are obtained from the Poisson equation, we solve (again, in a single computational block) the equation of continuity and the energy balance equation for holes. Finally, we correct the potential values by solving the Poisson equation with newly available values for the concentration and temperature of carriers. The whole procedure (illustrated in Fig. 4) is repeated until the required accuracy is achieved. In implementing coupled computational blocks (between the continuity and energy balance equations), the Jacobian of the linearised system of non-linear equations requires a special attention. For the electron subsystem, the Jacobian takes the form of the following matrix:

$$\boldsymbol{J}_e = \begin{pmatrix} \dfrac{\partial \vec{\mathcal{F}}^{\mathrm{n}}}{\partial \vec{n}} & \dfrac{\partial \vec{\mathcal{F}}^{\mathrm{n}}}{\partial \vec{T}_{\mathrm{n}}} \\ \dfrac{\partial \vec{\mathcal{F}}^{\mathcal{E}_{\mathrm{n}}}}{\partial \vec{n}} & \dfrac{\partial \vec{\mathcal{F}}^{\mathcal{E}_{\mathrm{n}}}}{\partial \vec{T}_{\mathrm{n}}} \end{pmatrix}. \tag{5.1}$$

The first (upper left) block of the Jacobian ($\partial \vec{\mathcal{F}}^{\mathrm{n}}/\partial \vec{n}$) is the same as in Section 3. The second (upper right) block $\partial \vec{\mathcal{F}}^{\mathrm{n}}/\partial \vec{T}_{\mathrm{n}}$ is determined by

$$\frac{\partial \mathcal{F}_i^{\mathrm{n}}}{\partial (T_{\mathrm{n}})_{i-1}} = \frac{\partial A_i^{\mathrm{n}}}{\partial (T_{\mathrm{n}})_{i-1}} n_{i-1}, \quad \frac{\partial \mathcal{F}_i^{\mathrm{n}}}{\partial (T_{\mathrm{n}})_i} = \frac{\partial C_i^{\mathrm{n}}}{\partial (T_{\mathrm{n}})_i} n_i, \quad \frac{\partial \mathcal{F}_i^{\mathrm{n}}}{\partial (T_{\mathrm{n}})_{i+1}} = \frac{\partial B_i^{\mathrm{n}}}{\partial (T_{\mathrm{n}})_{i+1}} n_{i+1}. \tag{5.2}$$

The third (lower left) block gives

$$\frac{\partial \mathcal{F}_i^{\mathcal{E}_{\mathrm{n}}}}{\partial n_{i-1}} = \tilde{A}_i^{\mathrm{n}} (T_{\mathrm{n}})_{i-1}, \quad \frac{\partial \mathcal{F}_i^{\mathcal{E}_{\mathrm{n}}}}{\partial n_i} = C_i^{\mathrm{n}} (T_{\mathrm{n}})_i + \frac{\partial R_i^{\mathcal{E}_{\mathrm{n}}}}{\partial n_i}, \quad \frac{\partial \mathcal{F}_i^{\mathcal{E}_{\mathrm{n}}}}{\partial n_{i+1}} = \tilde{B}_i^{\mathrm{n}} (T_{\mathrm{n}})_{i+1}, \tag{5.3}$$

and finally, the fourth (lower right) block of the matrix (5.1) is determined by

$$\frac{\partial \mathcal{F}_i^{\mathcal{E}_{\mathrm{n}}}}{\partial (T_{\mathrm{n}})_{i-1}} = \frac{\partial \tilde{A}_i^{\mathrm{n}}}{\partial (T_{\mathrm{n}})_{i-1}} (\mathcal{E}_{\mathrm{n}})_{i-1} + \tilde{A}_i^{\mathrm{n}} n_{i-1}, \quad \frac{\partial \mathcal{F}_i^{\mathcal{E}_{\mathrm{n}}}}{\partial (T_{\mathrm{n}})_i} = \frac{\partial \tilde{C}_i^{\mathrm{n}}}{\partial (T_{\mathrm{n}})_i} (\mathcal{E}_{\mathrm{n}})_i + \tilde{C}_i^{\mathrm{n}} n_i + \frac{\partial R_i^{\mathcal{E}_{\mathrm{n}}}}{\partial (T_{\mathrm{n}})_i}, \tag{5.4}$$

$$\frac{\partial \mathcal{F}_i^{\mathcal{E}_{\mathrm{n}}}}{\partial (T_{\mathrm{n}})_{i+1}} = \frac{\partial \tilde{B}_i^{\mathrm{n}}}{\partial (T_{\mathrm{n}})_{i+1}} (\mathcal{E}_{\mathrm{n}})_{i+1} + \tilde{B}_i^{\mathrm{n}} n_{i+1}. \tag{5.5}$$

The derivatives in relationships (5.2)–(5.5) are

$$\frac{\partial A_i^{\mathrm{n}}}{\partial (T_{\mathrm{n}})_{i-1}} = \frac{1}{h_{i-1}} \left[\frac{\partial D_{\mathrm{n}}}{\partial (T_{\mathrm{n}})_{i-1}} f(\lambda(\varphi, T_{\mathrm{n}})_i) - D_{\mathrm{n}} f'(\lambda(\varphi, T_{\mathrm{n}})_i) \frac{\lambda(\varphi, T_{\mathrm{n}})_i}{((T_{\mathrm{n}})_{i-1}^{l+1})} \right], \tag{5.6}$$

$$\begin{aligned} \frac{\partial B_i^{\mathrm{n}}}{\partial (T_{\mathrm{n}})_{i+1}} &= \frac{1}{h_{i+1}} \left[\frac{\partial D_{\mathrm{n}}}{\partial (T_{\mathrm{n}})_{i+1}} f_1(\lambda(\varphi, T_{\mathrm{n}})_{i+1}) - D_{\mathrm{n}} f_1'(\lambda(\varphi, T_{\mathrm{n}})_{i+1}) \frac{\lambda(\varphi, T_{\mathrm{n}})_{i+1}}{(T_{\mathrm{n}})_{i+1}^{l+1}} \right], \\ \frac{\partial C_i^{\mathrm{n}}}{\partial (T_{\mathrm{n}})_i} &= \frac{\partial A_i^{\mathrm{n}}}{\partial (T_{\mathrm{n}})_{i+1}} + \frac{\partial B_i^{\mathrm{n}}}{\partial (T_{\mathrm{n}})_{i-1}} \end{aligned} \tag{5.7}$$

and

$$\frac{\partial \tilde{A}_i^{\mathrm{n}}}{\partial (T_{\mathrm{n}})_{i-1}} = \frac{1}{h_{i-1}} \left[\beta_{\mathrm{n}} \frac{\partial D_{\mathrm{n}}}{\partial (T_{\mathrm{n}})_{i-1}} f(\lambda(\varphi, T_{\mathrm{n}})_i) - \tilde{\beta}_{\mathrm{n}} D_{\mathrm{n}} f'(\lambda(\varphi, T_{\mathrm{n}})_i) \frac{\lambda(\varphi, T_{\mathrm{n}})_i}{(T_{\mathrm{n}})_{i-1}^{l+1}} \right], \tag{5.8}$$

$$\begin{aligned} \frac{\partial \tilde{B}_i^{\mathrm{n}}}{\partial (T_{\mathrm{n}})_{i+1}} &= \frac{1}{h_{i+1}} \left[\beta_{\mathrm{n}} \frac{\partial D_{\mathrm{n}}}{\partial (T_{\mathrm{n}})_{i+1}} f_1(\lambda(\varphi, T_{\mathrm{n}})_{i+1}) - \tilde{\beta}_{\mathrm{n}} D_{\mathrm{n}} f_1'(\lambda(\varphi, T_{\mathrm{n}})_{i+1}) \frac{\lambda(\varphi, T_{\mathrm{n}})_{i+1}}{(T_{\mathrm{n}})_{i+1}^{l+1}} \right], \\ \frac{\partial \tilde{C}_i^{\mathrm{n}}}{\partial (T_{\mathrm{n}})_i} &= \frac{\partial \tilde{A}_i^{\mathrm{n}}}{\partial (T_{\mathrm{n}})_{i+1}} + \frac{\partial \tilde{B}_i^{\mathrm{n}}}{\partial (T_{\mathrm{n}})_{i-1}} \end{aligned} \tag{5.9}$$

where

$$\lambda(\varphi, T_{\mathrm{n}})_i = \frac{\varphi_i^{l+1} - \varphi_{i-1}^{l+1}}{(T_{\mathrm{n}})_{i-1}^{l+1}}.$$

The only term left to be determined is $R_i^{\mathcal{E}_{\mathrm{n}}}$:

$$R_i^{\mathcal{E}_{\mathrm{n}}} = -h_i^* \left\{ -\mu_{\mathrm{n}}[(T_{\mathrm{n}})_i] \varphi_{\check{x}\hat{x},i} - \frac{\mu_{\mathrm{n}}[(T_{\mathrm{n}})_i] (\varphi_{\check{x},i})^2}{(T_{\mathrm{n}})_i} + \frac{1}{\tau_\omega^{\mathrm{n}}[(T_{\mathrm{n}})_i]} - \frac{1}{(\tau_\omega^{\mathrm{n}}[(T_{\mathrm{n}})_i](T_{\mathrm{n}})_i)} \right\} (\mathcal{E}_{\mathrm{n}})_i, \tag{5.10}$$

where the normalised functions $\mu_{\rm n}$ and $\tau_\omega^{\rm n}$ are given in the form: $\mu_{\rm n}[(T_{\rm n})_i] = \mu_{\rm n}^0\sqrt{(T_{\rm n})_i}$ and $\tau_\omega^{\rm n} = 1.5\mu_{\rm n}^0\sqrt{(T_{\rm n})_i}/(v_{\rm s}^{\rm n})^2$. Hence,

$$R_i^{\mathcal{E}_{\rm n}} = h_i^* \left(\mu_{\rm n}^0 (T_{\rm n})_i^{1.5} \varphi_{\bar{x}\hat{x},i} + \mu_{\rm n}^0 \sqrt{(T_{\rm n})_i} (\varphi_{\check{x},i})^2 + \frac{2(1-(T_{\rm n})_i)(v_{\rm s}^{\rm n})^2}{3\mu_0^{\rm n}\sqrt{(Tn)_i}} \right) n_i \tag{5.11}$$

and

$$\frac{\partial R_i^{\mathcal{E}_{\rm n}}}{\partial (T_{\rm n})_i} = h_i^* \left(1.5\mu_{\rm n}^0 \sqrt{(T_{\rm n})_i} \varphi_{\bar{x}\hat{x},i} + \frac{\mu_{\rm n}^0}{2\sqrt{(T_{\rm n})_i}} (\varphi_{\check{x},i})^2 - \frac{(1+(T_{\rm n})_i)(v_{\rm s}^{\rm n})^2}{3\mu_0^{\rm n}(T_{\rm n})_i^{3/2}} \right) n_i . \tag{5.12}$$

Finally, in this section we provide results of computational experiments with the quasi-hydrodynamic model. All computations have been performed for 2^{10} grid points and this value was set as the default. The first group of experiments was designed for the ballistic diode (see Fig. 1(b)). The distributions of concentrations, potential and temperature along the semiconductor structure for the two different applied voltages, $V = 0.1$ and 0.5 V, are given in Figs. 5–7 respectively. In Fig. 8, we provide the profile of electron velocity and in Fig. 9, the Mach number (computed as the ratio $v_{\rm n}/\sqrt{5T_{\rm n}/(3m_{\rm n})}$, where $m_{\rm n}$ is the effective electron mass) is displayed.

The second group of experiments was conducted for a bipolar-type of devices, the PIN diode (see Fig. 1(a)). In Figs. 10–14, we present the computed distributions of the potential as well as concentrations

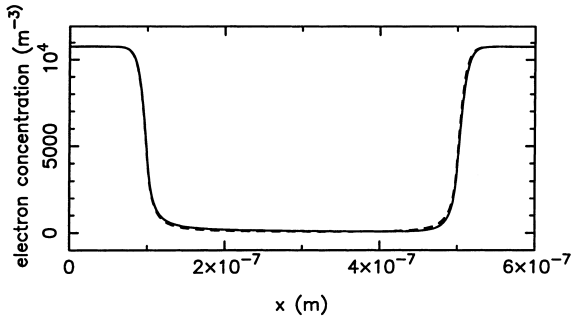

Fig. 5. Concentration of electrons in normalised unit. Applied voltages are 0.1 V (dashed line) and 0.5 V (solid line).

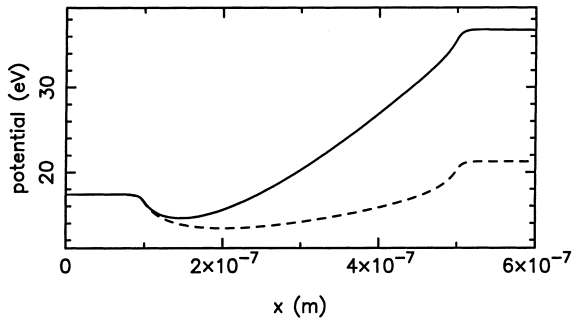

Fig. 6. Potential profile in normalised unit. Applied voltages are 0.1 V (dashed line) and 0.5 V (solid line).

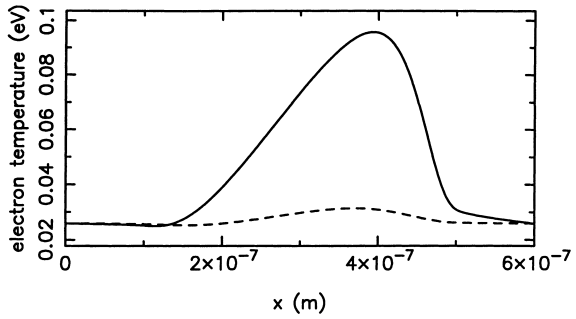

Fig. 7. Temperature distributions of electrons in unit eV. Applied voltages are 0.1 V (dashed line) and 0.5 V (solid line).

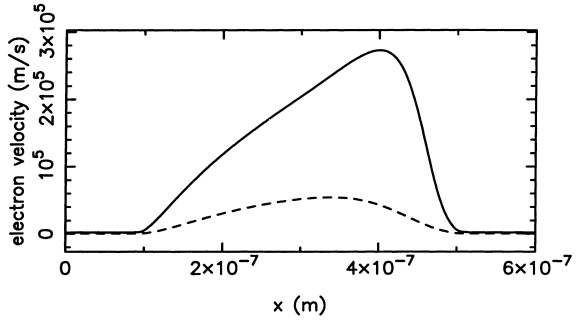

Fig. 8. Velocity distributions of electrons in unit m/s. Applied voltages are 0.1 V (dashed line) and 0.5 V (solid line).

and temperatures of carriers for this device. Plots of electron velocity and of the Mach number are given in Figs. 15 and 16, respectively. A high, narrow velocity peak and a narrow area where the Mach number is greater than one, suggest that the quasi-hydrodynamic model may overestimate some physical characteristics of the devices. Similar effects were previously reported in the literature [1,2].

We note that PIN diodes can work in both forward and reverse biased regimes. In the forward-bias case these devices exhibit a very low RF resistance, a higher conductivity and a larger breakdown than standard PIN diodes. As can be seen from Figs. 10–14, deviations of carrier temperature away from equilibrium

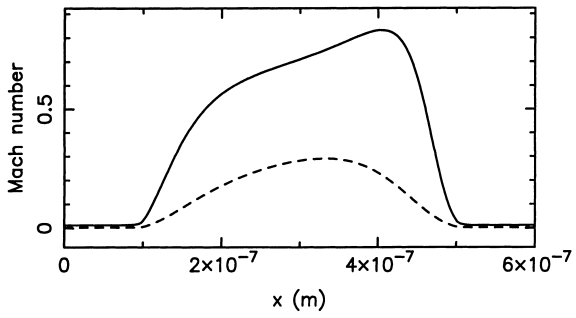

Fig. 9. Mach number of electrons. Applied voltages are 0.1 V (dashed line) and 0.5 V (solid line).

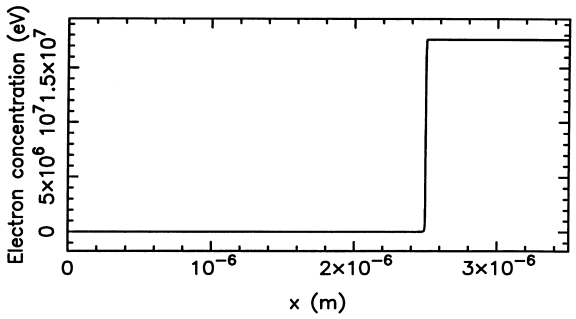

Fig. 10. Concentration of electrons in normalised unit. Applied voltages are −0.5 V (dashed line), 0. V (solid line), and 0.05 V (dash-dotted line).

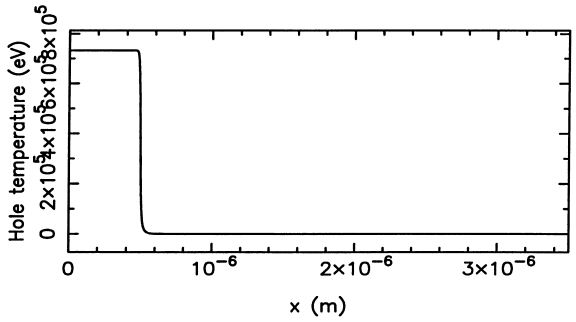

Fig. 11. Concentration of holes in normalised unit. Applied voltages are −0.5 V (dashed line), 0. V (solid line), and 0.05 V (dash-dotted line).

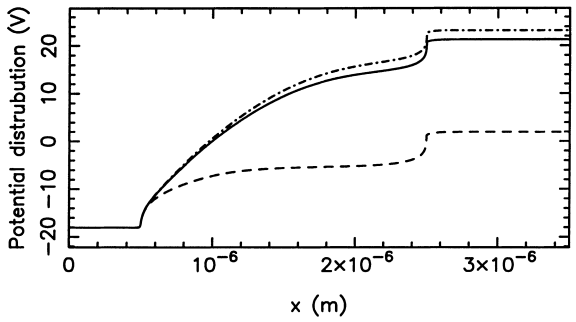

Fig. 12. Potential profile in normalised unit. Applied voltages are −0.5 V (dashed line), 0. V (solid line), and 0.05 V (dash-dotted line).

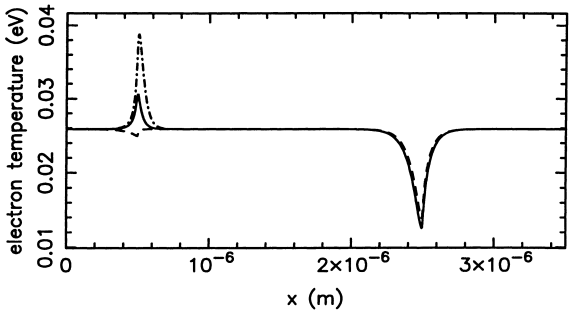

Fig. 13. Temperature distributions of electrons in unit eV. Applied voltages are −0.5 V (dashed line), 0. V (solid line), and 0.05 V (dash-dotted line).

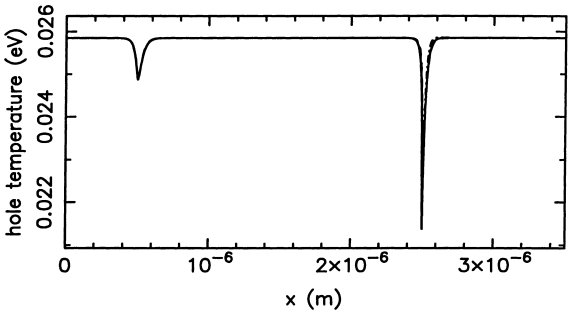

Fig. 14. Temperature distributions of holes in unit eV. Applied voltages are −0.5 V (dashed line), 0. V (solid line), and 0.05 V (dash-dotted line).

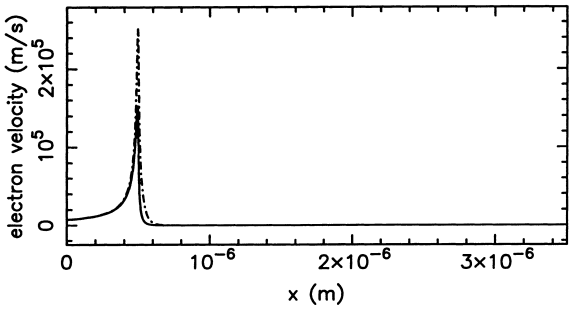

Fig. 15. Velocity distributions of electrons in units m/s. Applied voltages are 0. V (solid line) and 0.05 V (dash-dotted line).

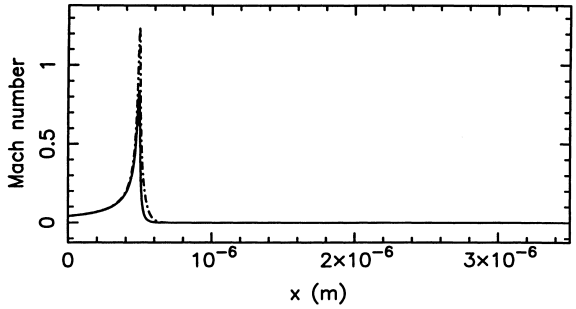

Fig. 16. Mach number of electrons. Applied voltages are 0. V (solid line) and 0.05 V (dash-dotted line).

values do not have a significant influence on the main characteristics of the device. This may not be the case in the reverse-bias condition [4].

Acknowledgements

Authors were supported by grant USQ-PTRP 17989 and by Australian Research Council Small Grant 17906. We thank Tim Passmore for his assistance at the final stage of preparation of this paper.

References

[1] Y. Apanovich, E. Lyumkis, Polsky et al., Steady-state and transient analysis of submicron devices using energy balance and simplified hydrodynamic models, IEEE Trans. Computer-Aided Design Integrated Circuits Syst. 13 (6) (1994) 702–711.
[2] C.L. Gardner, J.W. Jerome, D.J. Rose, Numerical methods for the hydrodynamic device model: subsonic flow, IEEE Trans. Computer-Aided Design 8 (5) (1989) 501–507.
[3] D. Kakati, C. Ramanan, V. Ramamurthy, Numerical analysis of electrophysical characteristics of semiconductor devices accounting for the heat transfer, in: J.J.H. Miller (Ed.), NEMACODE IV: Proceedings of the Fourth International Conference on the Numerical Analysis of Semiconductor Devices and Integrated Circuits, Trinity College, Dublin, Ireland, Bool Press, Dublin, 1985, pp. 326–331.
[4] R.V.N. Melnik, K.N. Melnik, Modelling of nonlocal physical effects in semiconductor plasma using quasi-hydrodynamic models, in: J. Noye, M. Teubner, A. Gill (Eds.), Computational Techniques and Applications: CTAC97, World Scientific, Singapore, 1998, pp. 441–448.
[5] A.A. Samarskii, Theorie der Differenzenverfahren, Mathematik und ihre Anwendengen in Physik und Technik, Aufl. Leipzig, Academische Verlagesellschaft Geest & Portig, 1984.
[6] A.A. Samarskii, E.S. Nikolaev, Numerical Methods for Grid Equations, Birkhauser Verlag, Basel, Boston, 1989.